Available online at www.sciencedirect.com
SCIENCE DIRECT®
International Journal of Heat and Mass Transfer 49 (2006) 97–107
International Journal of HEAT and MASS TRANSFER
www.elsevier.com/locate/ijhmt

Multi-length and time scale thermal transport using the lattice Boltzmann method with application to electronics cooling

Rodrigo A. Escobar [a,c], Sartaj S. Ghai [b], Myung S. Jhon [b,*], Cristina H. Amon [a]

[a] Department of Mechanical Engineering and Institute for Complex Engineered Systems, Carnegie Mellon University, Pittsburgh, PA 15213, USA
[b] Department of Chemical Engineering and Institute for Complex Engineered Systems, Carnegie Mellon University, Pittsburgh, PA 15213, USA
[c] Departamento de Ingeniería Mecánica y Metalúrgica, Pontificia Universidad Católica de Chile, Santiago, Chile

Received 2 December 2004; received in revised form 4 August 2005
Available online 20 December 2005

Abstract

The lattice Boltzmann method (LBM) is used to investigate one-dimensional, multi-length and -time scale transient heat conduction in crystalline semiconductor solids, in which sub-continuum effects are important. The implementation of this method and its application to electronic devices are described. A silicon-on-insulator transistor subject to Joule heating conditions is used as a case study to illustrate the essence of the LBM. We compare our LBM results, for the diffusive to the ballistic transport regimes, with various hierarchical methodologies of heat transport such as the Fourier, Cattaneo, and ballistic-diffusive transport equations.

Keywords: Lattice Boltzmann method; Nanoscale heat transfer; Silicon-on-insulator transistor; Hotspots; Electronics cooling

1. Introduction

As the characteristic dimensions of electronic devices become smaller, the ability to model sub-continuum energy transfer effects has become increasingly important. It is now well established that the continuum-based Fourier equation of heat conduction leads to erroneous results when the mean free path of the heat carriers becomes comparable, or larger, than the characteristic length of the domain of interest [1]. In addition, Fourier law assumes an instantaneous heat propagation, which leads to significant errors in the thermal predictions as the time scale of interest becomes comparable or smaller than the relaxation time of the heat carriers [2]. It has been reported that for crystalline semiconductor devices, acoustic phonons, which are quantized lattice vibrations, are the dominant energy carriers at the room temperature. Under the gray model, which considers a linear dispersion relationship with a single propagating mode, following the Debye assumption, the phonon mean free path, Λ, and relaxation time, τ_r, for silicon are computed to be 41 nm and 6.5 ps respectively. The phonon group velocity, v can be obtained from the slope of the dispersion relation, and is 6400 m/s. The phonon mean free path and relaxation time are related by the phonon group velocity (v) as $\Lambda = v\tau_r$. When considering a semi-gray model, with one propagating (acoustic) mode

* Corresponding author. Tel.: +1 412 268 2233; fax: +1 412 268 7139.
E-mail address: mj3a@andrew.cmu.edu (M.S. Jhon).

0017-9310/$ - see front matter © 2005 Elsevier Ltd. All rights reserved.
doi:10.1016/j.ijheatmasstransfer.2005.08.003

Nomenclature

b	hotspot width, m
c	phonon velocity, m/s
d	number of lattice directions
D_p	phonon density of states per unit volume, m^{-3}
e	phonon energy density, J m^{-3}
e^0	equilibrium phonon energy density, J m^{-3}
f	phonon distribution function
f^0	equilibrium phonon distribution function
g_{e-p}	phonon generation rate due to electron–phonon scattering
$\hbar$	Planck constant divided by 2π, J s^{-1}
k	thermal conductivity, W m^{-1} K^{-1}
k_b	Boltzmann constant, J K^{-1}
Kn	Knudsen number, Λ/L
l	length, m
L	characteristic length, m
p	polarization
q	heat flux, W m^{-2}
q_v	heat generation rate per unit volume, W m^{-3}
t	time, s
t^*	dimensionless time, t/τ
T	absolute temperature, K
v	phonon group velocity, m/s
W	grid weight factor
X^*	dimensionless length

Greek symbols

θ_D	Debye temperature of solid, K
η	number density of oscillators
Λ	phonon mean free path, m
λ	phonon wavelength, m
σ	Stefan–Boltzmann constant, J s^{-1} m^{-2} K^{-4}
τ_c	phonon collision time, s
τ_r	phonon relaxation time, s
ω	phonon frequency, Hz

Subscripts

c	collision
i	direction
p	polarization
r	relaxation
w	wall
x, y, z	directions

Superscripts

0	equilibrium
*	dimensionless

and one reservoir (optical) mode, the phonon mean free path Λ is computed to be 300 nm, and the phonon relaxation time τ_r to be 70 ps . Current transistor technology, for example, is yielding devices with channel lengths within the 90 nm technology node, and even smaller channel lengths (65 nm technology node) are in the development phase [3]. Even when the actual values of Λ and τ_r are still a subject of discussion [4–6], it is clear that phonon transport in sub-micron semiconductor structures is likely to be within the sub-continuum regime and, therefore, more accurate and consistent models for phonon transport are needed. An example of an electronic device where sub-continuum thermal effects are important are the transistors built with the silicon-on-insulator (SOI) technology, where a thin silicon layer is deposited on top of a silicon dioxide layer, which allows faster device switching speeds due to the reduced capacitive coupling with the substrate [5,6]. The high electric field strengths generated within the device accelerate the electrons, which interact with high-energy phonons, transferring their energy mainly to the optical branch of phonons. Very slow propagation speed of optical phonons prevents the thermal energy from leaving the electron–phonon interaction zone. These high-energy optical phonons decay to faster propagating acoustic phonons that transport thermal energy away from the interaction zone. As the timescale of the electron–phonon scattering process is much faster than the decay from optical to acoustic modes, local non-equilibrium conditions arise, which directly translate into a hotspot region that displays higher temperature levels than those predicted by the continuum-based Fourier equation. The dimensions of this hotspot zone (on the order of 10–30 nm) have been reported to be smaller than the phonon mean free path, therefore rendering Fourier law inapplicable [5–7]. In addition, the silicon dioxide layer has poor thermal conductivity and, as a result, most of the heat generated within the SOI device remains confined to the thin silicon film, making it susceptible to thermal failure under electrostatic discharge (ESD) events or even under normal switching activity during continuous operation [5,6]. Since sub-continuum heat conduction phenomena are very difficult to measure directly, numerical simulations begin to play a critical role in the thermal design and management of semiconductor nanostructures.

Fig. 1 provides schematics for the computational techniques used to predict thermal transport in solids, and their range of applicability for length and time scales [1,7–9]. The Fourier equation of heat conduction is valid only when the characteristic length, L, of the device is larger than the Λ by an order of magnitude

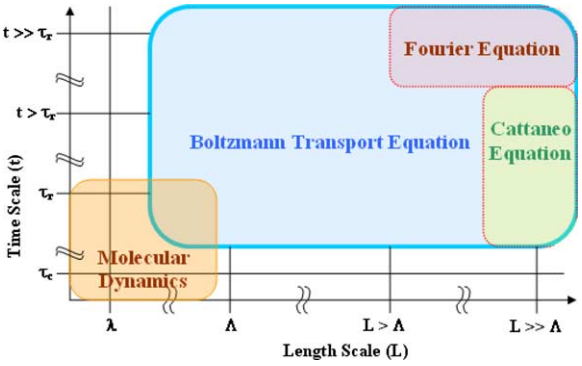

Fig. 1. Range of applicability of different computational techniques in heat conduction as function of length and time scales.

or more, and when the time scale of the process, t, is much larger than τ_r, which is the time required to obtain local thermodynamic equilibrium after a thermal perturbation is introduced into the phonon system. For shorter time scales, on the order of the τ_r, and length scales much larger than the Λ, the Cattaneo equation is constructed by introducing a time delay between the applied heat flux and the resulting temperature gradient. However, these equations are limiting cases of the Boltzmann transport equation (BTE). They may not be able to simulate multi-length and -time scale phenomenon as required for an accurate thermal simulation of microelectronic devices. The BTE with the single relaxation time approximation [10–15] can be used to simulate energy transport in the sub-continuum regime, as long as the particle assumption for the heat carriers is valid; that is, whenever the timescale is longer than the collision time, τ_c, and the L is larger than the phonon wavelength, λ. When L is on the order of λ, and time scales are of the order of the collision time τ_c, we can no longer assume that the particle nature of phonons is valid, and have to perform molecular dynamics simulations for the device. In general, extensive computational effort is required to solve the BTE, since it involves seven independent variables descriptive for space, time, and momentum or velocity domain [10,11]. This has led to the development of the lattice Boltzmann method (LBM) that, in essence, discretizes the BTE, maintaining its accuracy while reducing the computational effort necessary to solve it [12–15]. The inherent transient nature, reduced computational effort when compared to BTE solutions, and the ability to capture the complex physics of phonon transport, make the LBM an attractive approach to describe the complex multi-scale phenomena of energy transport in electronic devices. In this paper, first we will present the derivation of the LBM from the BTE. Then, we will use the LBM to study sub-continuum heat conduction in thin films and small-scale electronic devices (e.g., transient thermal response of a simplified model of an SOI device subject to a heat generation pulse). Finally, we will compare the LBM predictions with those obtained by the hierarchical equations in heat conduction.

2. BTE for phonons

The BTE for phonons under the BGK approximation is [10–15]:

$$\frac{\partial f}{\partial t} + \mathbf{v}\cdot\nabla f = \frac{f^0 - f}{\tau_r} + g_{e\text{–}p}, \tag{1}$$

where f is the phonon distribution function, $\mathbf{v}$ is the phonon group velocity, $g_{e\text{–}p}$ is the phonon generation rate due to electron–phonon scattering, and f^0 is the equilibrium distribution function given by the Bose–Einstein statistics [16,17]

$$f^0 = \frac{1}{e^{(\hbar\omega/k_b T)} - 1}, \tag{2}$$

where $\hbar$ is the Planck constant (h) divided by 2π, ω is the phonon frequency, k_b is the Boltzmann constant, and T is the absolute temperature. In order to take advantage of the simplifying assumptions of the Debye model, the BTE can be cast into an equation for the phonon energy density, e, by integrating it over the frequency spectrum as

$$e(T) = \sum_p \int f \hbar\omega_p D_p(\omega)\, d\omega, \tag{3}$$

where p is the polarization of phonons (acoustic and optical) and $D_p(\omega)$ is the phonon density of states per unit volume. For simplicity, we neglect the effects of temperature on the dispersion relations and the phonon density of states in this paper. Then, the BTE in a phonon energy density (e) formulation is given by

$$\frac{\partial e}{\partial t} + \mathbf{v}\cdot\nabla e = -\frac{e - e^0}{\tau_r} + q_v, \tag{4}$$

where e^0 is the equilibrium phonon energy density and q_v is the internal heat generation rate per volume [11,12]. In a one-dimensional analysis, Eq. (4) becomes

$$\frac{\partial e}{\partial t} + v_x\frac{\partial e}{\partial x} = -\frac{e - e^0}{\tau_r} + q_v, \tag{5}$$

where v_x is the component of velocity along the x-axis. Under non-equilibrium conditions, the conventional definition of temperature is no longer valid [7,8]. Therefore, we must resort to an alternative temperature definition, in which the total energy of phonons at a given lattice point is equal to the total equilibrium phonon energy at the equivalent equilibrium temperature. The relation between phonon energy and lattice temperature is obtained by using the Debye model [16,17], which essentially collapses all phonon branches into a single,

linear dispersion relation with one phonon propagation speed, and is given by

$$e(T) = \left(\frac{9\eta k_b}{\theta_D^3}\int_0^{\theta_D/T}\frac{z^3}{e^z-1}dz\right)T^4, \tag{6}$$

where θ_D is the Debye temperature of the solid and $\eta = \frac{1}{6\pi^2}\left(\frac{k_b\theta_D}{\hbar\omega}\right)^3$ is the number density of oscillators.

3. The gray LBM

The BTE is described in continuous variables such as the space, time, and velocity. As a discrete representation of the BTE, the LBM [18] discretizes the space domain by defining lattice sites where the phonon energy density is calculated. The three main components of the LBM include the lattice, the lattice Boltzmann kinetic equation (LBKE), and the site-to-site transport restriction. The lattice is a network of discrete points arranged in a regular mesh, as shown in Fig. 2. Phonons residing in a particular lattice site propagate only to a neighboring lattice site by ballistically traveling at a speed of $\boldsymbol{c}$, which is given by the phonon velocity obtained from the Debye model, and collide with phonons residing at the neighboring lattice site. Since the phonons can travel in the positive or negative direction along a specific axis on the lattice, we introduce the subscript i to the various phonon parameters, in order to differentiate between the discrete values associated with each propagation direction. The temporal domain is also discretized by restricting the phonons to travel from one lattice site to the neighboring lattice site in a definite time step, which corresponds to the site-to-site transport restriction. The velocity domain is also discretized by allowing only a discrete set of propagation velocities $\boldsymbol{c}_i$ $(i = 1,2,3,4)$ in the main lattice directions. In Fig. 2, $\boldsymbol{c}_1 = (c,0)$ and $\boldsymbol{c}_2 = (-c,0)$ represent the velocities in the horizontal direction, while $\boldsymbol{c}_3 = (0,c)$ and $\boldsymbol{c}_4 = (0,-c)$ correspond to the vertical direction. It is worth mentioning that the LBM is not only a discretized BTE, but also a numerical scheme on its own. The LBM is used to compute the thermal state of phonons at each discrete node, at every time step based on simple kinetic equations, which makes the incorporation of additional physics into the system a relatively easy task.

To derive the LBKE from the BTE, the time and space derivatives in Eq. (5), are discretized as

$$\frac{\partial e}{\partial t} = \frac{e(x,t+\Delta t)-e(x,t)}{\Delta t} \quad \text{and} \quad \frac{\partial e}{\partial x} = \frac{e(x+\Delta x,t+\Delta t)-e(x,t+\Delta t)}{\Delta x}, \tag{7}$$

where Δx and Δt are the lattice spacing or site-to-site distance and the discrete time step, respectively. Then, we substitute Eq. (7) into Eq. (5) and use directionality subscripts for each direction in the lattice, to get

$$\frac{e_i(x,t+\Delta t)-e_i(x,t)}{\Delta t} + c_i\frac{e_i(x+\Delta x,t+\Delta t)-e_i(x,t+\Delta t)}{\Delta x} = -\frac{e_i(x,t)-e_i^0(x,t)}{\tau_r} + q_v. \tag{8}$$

As the phonons are constrained to travel only from a lattice site to the neighboring lattice site, we define the time step-lattice spacing relation to be $\Delta x = c_i\Delta t$. The lattice spacing, and therefore the time step magnitude are chosen, based on accuracy constraints, in order to get a mesh-independent solution. In general, a lattice spacing smaller than the phonon mean free path, and a time step shorter than the phonon relaxation time are recommended. The site-to-site transport restriction allows Eq. (8) to be expressed as a discrete propagation equation with internal heat generation equation

$$e_i(x+\Delta x,t+\Delta t) - e_i(x,t) = -\frac{\Delta t}{\tau_r}\left[e_i(x,t)-e_i^0(x,t)\right] + \Delta t q_v. \tag{9}$$

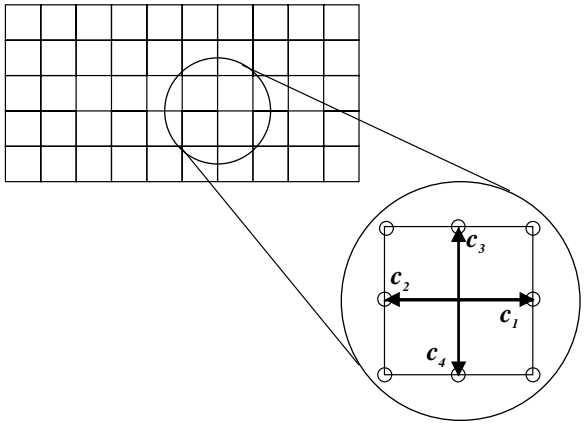

Fig. 2. Two-dimensional lattice and velocity vectors in a square lattice.

Rearranging Eq. (9) and defining the grid weight factor $W_i \equiv \Delta t/\tau_r$, same for all lattice directions, we get the LBKE that governs the dynamics of phonons in the lattice as

$$e_i(x+\Delta x, t+\Delta t) = (1-W_i)e_i(x,t) + W_i e_i^0(x,t) + \Delta t q_v, \tag{10}$$

where the term $e_i(x,t)$ corresponds to the discrete phonon energy density, which is proportional to the population of phonons associated with a specific direction in the lattice. The total phonon energy density is defined as the sum of discrete phonon energy densities over all the lattice directions, d,

$$e(x,t) = \sum_{i=1}^{d} e_i(x,t). \tag{11}$$

Assuming isotropy, the equilibrium phonon energy density is considered to be same in all lattice directions and can be obtained from Eq. (11):

$$e_i^0(x,t) = e(x,t)/d. \tag{12}$$

Eq. (10) is solved at each lattice site to obtain e_i, and then temperature distribution is obtained from Eq. (6).

The LBM algorithm can be summarized as

1. Set an initial temperature to find the initial phonon energy density at each lattice site from Eq. (6).
2. Determine the directional, discrete phonon energy density at each lattice site for all lattice directions by using Eq. (12).
3. Apply Eq. (10) to all lattice sites and directions to allow phonon propagation and collision.
4. Use Eqs. (11) and (12) to determine the new phonon energy density at each lattice site.
5. Use Eq. (6) to find the lattice temperature.
6. Repeat steps 3 and 4 until desired time for simulation is achieved.

4. Boundary conditions

To impose temperature boundary conditions, Eq. (6) is used to find the phonon energy density that corresponds to the desired temperature level. This value of energy density is imposed to the boundary nodes, which are then assumed to be in thermodynamical equilibrium conditions. Energy densities for the specific direction at the boundary nodes are obtained from Eq. (12). In addition, heat flux can be obtained by [2],

$$q_i = \sum_p v_i f \hbar\omega D_p(\omega)\,\mathrm{d}\omega = \sum_p v_i e_i. \tag{13}$$

Observing that v_i is constant, Eq. (13) can be considered as the product of the phonon group velocity and the phonon energy density. In the gray approach, it is assumed that only the longitudinal acoustic phonons contribute significantly to the heat conduction, thus the summation can be simplified to include that specific polarization only. In one-dimensional geometry, the relation between discrete directional phonon energy density and the net heat flux becomes:

$$e_1(x,t) = \frac{q_1}{v_1} + e_2(x,t). \tag{14}$$

Extending this formulation to higher dimensions is straightforward, and the general expression for the heat flux can be written as

$$q_i = \sum_{j=1}^{d} v_i \cdot e_j(x,t). \tag{15}$$

5. Results

We will first examine heat transport across a thin film for different length and time scales. Then, a simplified model of an SOI transistor will be examined. Finally, a comparison between the results obtained via the LBM and other methodologies will be presented.

5.1. One-dimensional heat transport across a thin film

Here, we consider one-dimensional heat transport across a thin film of thickness L as an example. The phonon parameters are those of a gray model (Section 1), that is, phonon group velocity of 6400 m/s, a phonon mean free path of 41 nm, and a phonon relaxation time of 6.53 ps. The initial temperature of the film is taken to be T_{w1}. At time $t^* = 0$ the right face of the film is kept at T_{w1} while the left face is set at a higher temperature T_{w2}. Fig. 3 shows the dimensionless steady-state temperature profiles in this film as calculated via the LBM for a broad range of Knudsen numbers, $Kn = \Lambda/L$. Here, dimensionless length is $X^* = x/L$ and dimensionless temperature is $T^* = (T - T_{w1})/(T_{w2} - T_{w1})$. In the diffusive limit, where Kn is very small ($Kn \leqslant 0.1$), the temperature profile is linear (as predicted by the Fourier equation). As Kn increases, a temperature slip appears at both boundaries and a linear profile exists inside the film, which is a characteristic behavior in the transitional (between diffusive and ballistic) energy transfer regime. As Kn further increases, the phonon transport processes become ballistic and the temperature profile becomes almost flat inside the film, displaying significant temperature slip at both boundaries. These steady-state results are in excellent agreement with those of Majumdar [2], Zhang and Fisher [12], and Narumanchi et al. [10,11].

The transient temperature profiles in a film in the diffusive regime ($Kn = 0.001$) are shown in Fig. 4(a). The simulations are performed for a range of dimensionless

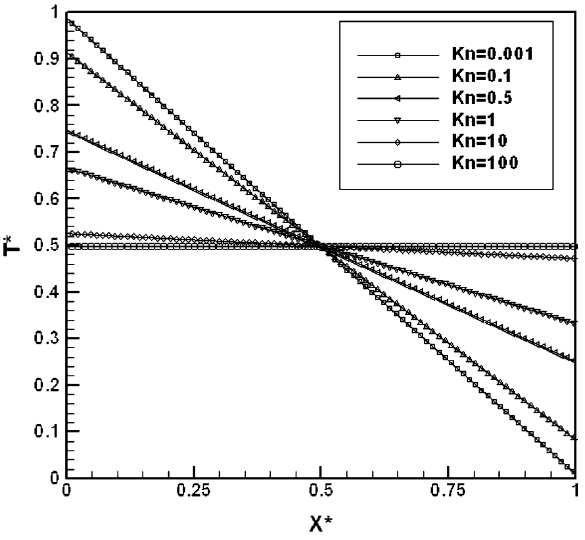

Fig. 3. Dimensionless steady-state temperature distributions in a thin film.

time $t^* \equiv t/\tau_r$, where t is the total time of the simulation. It is observed that our result agrees very well with the analytical solution of the Fourier equation. This agreement will be thoroughly analyzed and demonstrated in the following section. As time progresses, the temperature profile reaches a steady-state linear profile. This behavior is characteristic of diffusive heat transfer, and is in excellent agreement with Fourier law.

Fig. 4(b) depicts transient temperature profiles in a thin film for the transitional regime ($Kn = 1$). Unlike the diffusive regime case (Fig. 4(a)), discontinuous temperature slip conditions appear at the boundaries and the transient temperature profile inside the medium travels like a wave with a discontinuous wavefront propagating at the phonon group velocity (6400 m/s). The temperature profiles inside the medium between the boundary and the propagating wavefront are linear. Therefore, at Kn on the order of unity, both the ballistic effects, characterized by temperature jumps at the boundaries, and the diffusive effects, characterized by a linear temperature drop inside the film are observed.

Fig. 4(c) shows transient temperature profiles in the ballistic regime characterized by a high Kn ($Kn = 10$), where it is observed that a temperature slip occurs at the boundary, as in the transitional regime. The propagating heat wave gives origin to an almost flat temperature profile inside the film as it travels towards the cold boundary because the phonons does not get enough chance to undergo collisions to dissipate energy and establish thermal equilibrium. A steady state is established once the heat wave reaches the cold boundary.

In summary, the transition from diffusive to ballistic heat transport in thin films is characterized by the pres-

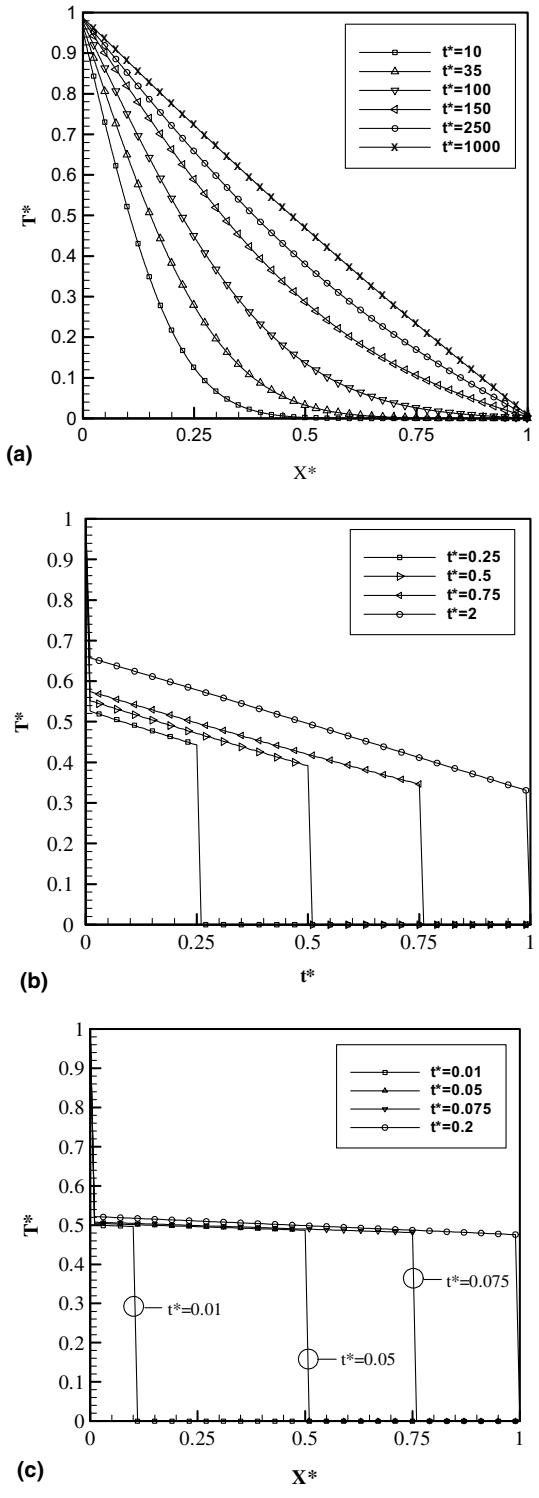

Fig. 4. Transient temperature profiles in a thin film for (a) $Kn = 0.001$ (diffusive regime); (b) $Kn = 1$ (transitional regime); and (c) $Kn = 10$ (ballistic regime).

ence of discontinuous temperature profiles at each boundary of the thin film, and the wave-like propagation of thermal energy. It is important to discuss the physical meaning of the imposed boundary conditions. The constant temperature levels at the boundaries have the net effect of enforcing an emission of phonons at energy level corresponding to the boundary temperature. As we approach the sub-continuum regime, phonons traveling to the boundary have a significantly different energy level than that of the phonons emitted from the boundary. This difference in energy level results in a non-equilibrium state inside the thin film, with the consequence of strong scattering effects and increased gradients in the total energy level of the phonon system, which results in the temperature slip at the boundaries. This slip, occurs at a length scale comparable to the phonon mean free path (its magnitude depends on the *Kn*), has also been well documented theoretically for the rarified gas dynamics.

5.2. A simplified SOI device

In this section, we model the SOI as a one-dimensional silicon thin film of length L. The hotspot is modeled by imposing a source term on a region of width b, centered in the silicon layer, as shown in Fig. 5, where the ratio b/L is equal to 0.01. The LBKE is solved in this domain, using the constant temperature boundary conditions (300 K) at both ends. The initial condition is a constant temperature distribution of 300 K for all lattice sites. At the beginning of the simulation, a constant heat pulse is applied for a period of dimensionless time t_q^* defined as $t_q^* \equiv t_q/\tau_r$, where t_q is the heat pulse duration, and τ_r is the phonon relaxation time. The left boundary is located at a dimensionless location $X^* = 0$, and the right boundary at $X^* = 1$, where the dimensionless length is given by $X^* = x/L$. The transport regime is characterized in terms of the *Kn*. For a *Kn* smaller than 1, the transport regime is located within the diffusive regime, for a *Kn* on the order of 1, the transport regime becomes transitional, and a *Kn* much larger than 1 represents a ballistic transport regime. The dimensionless temperature is defined as $T^* = (T - T_w)/(T_{max} - T_w)$, where T_w is the temperature at both boundaries and T_{max} is the maximum temperature level inside the hotspot.

The dimensions and parameters used in the SOI simulation are the same as those used in the thin film simulation section, with domain lengths such as to provide a *Kn* range from 0.01 to 10, which covers the diffusive, transitional, and ballistic regimes.

The time evolution of the temperature profile for the gray LBM in the diffusive regime ($L = 4100$ nm, $Kn = 0.01$) is shown in Fig. 6(a). The total time of the simulation is set to $t^* = 60$, with a pulse duration of $t_q^* = 0.6$. For $t^* = 0.6$, just before the heat pulse is turned off, the temperature profile inside the hotspot region shows the maximum temperature rise. As time elapses, the temperature profile broadens and the peak temperature rapidly decreases, characteristically similar to that of the heat diffusion process. This result agrees very well with the results presented by Narumanchi et al. [10] for the transient thermal response of an SOI.

The zone between the hotspot and the boundaries displays the characteristic shape of transient heat conduction. The phonon mean free path Λ is much smaller than the film thickness L, and therefore, the resulting *Kn* is smaller than 1. This implies that temperature slip effects are not significant, and thus, a non-vanishing temperature gradient can be defined at the boundary. Fourier law, therefore, can be used to calculate the total heat flux leaving the domain.

Decreasing the domain length by two orders of magnitude, where the Λ has a comparable magnitude to that of the film thickness L, marches the system into the transitional regime. For a domain length of $L = 41$ nm, $Kn = 1$ (Fig. 6(b)). The total time of the simulation is set to $t^* = 0.6$, with a pulse duration of $t_q^* = 0.006$. Here, the temperature profile for $t^* = 0.006$ depicts a maximum value at the hotspot center, and a linear evolution with time as the energy travels away from the heated region. As the time evolves, the temperature profile displays a strong wave nature, with high temperature zones traveling away from the hotspot, while the temperature decreases to an equilibrium level, that is, higher than the initial temperature at the central region, but

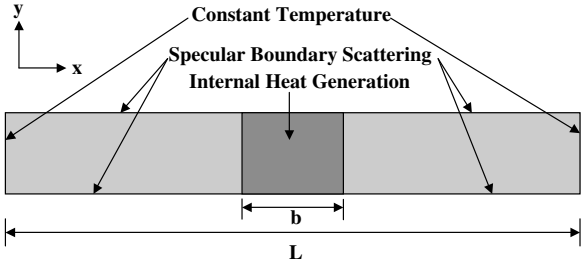

Fig. 5. Schematic of an SOI device.

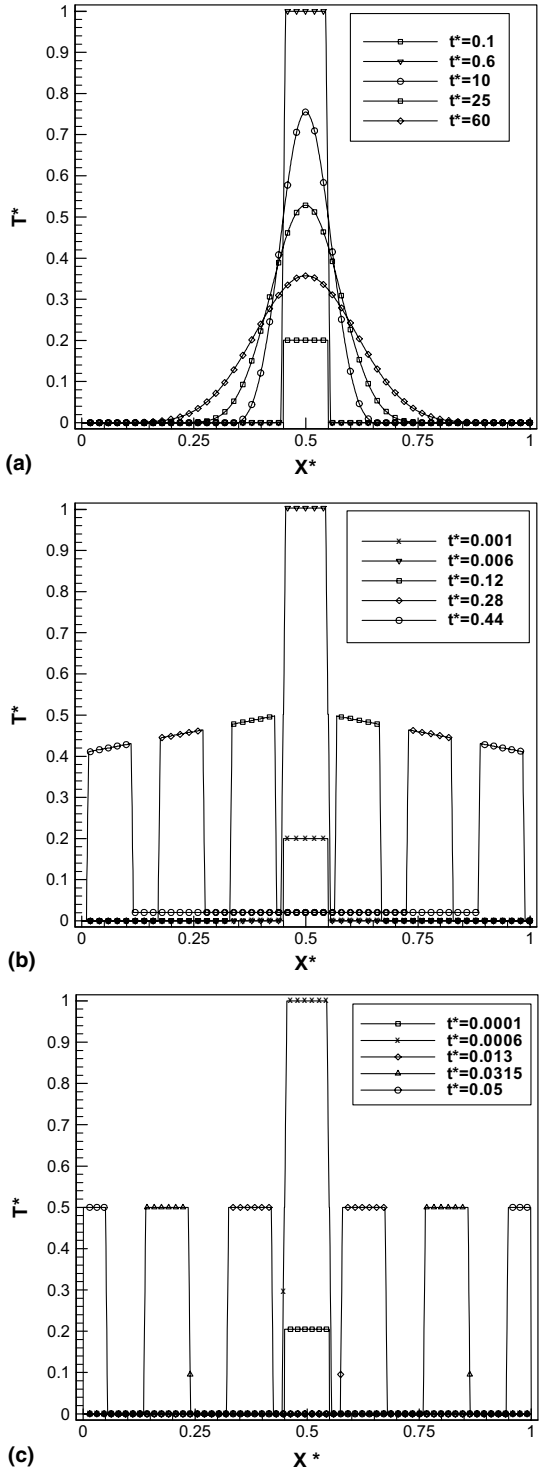

Fig. 6. Transient temperature profiles in one-dimensional SOI device for $v = 6400$ m/s and (a) $Kn = 0.01$ (diffusive regime) with heat pulse duration $t_q^* = 0.6$; (b) $Kn = 1$ (transitional regime) with heat pulse duration $t_q^* = 0.006$; and (c) $Kn = 1$ (ballistic regime) with heat pulse duration $t_q^* = 0.0006$.

significantly lower than the wavefront temperatures which itself decreases by losing some energy to the domain it travels. Finally, as the wavefront reaches the boundary, a temperature slip characteristic of transitional and ballistic regimes develops. Since the temperature gradient at both boundaries is undefined, Fourier law is not valid, and therefore, the heat flux must be calculated via Eq. (14).

As the Kn increases by another order of magnitude ($Kn = 10$), a fully ballistic regime is obtained. The total time of the simulation is set to $t^* = 0.06$, with a pulse duration of $t_q^* = 0.0006$. Fig. 6(c) shows that the energy travels in waves away from the hotspot with a nearly constant wavefront peak temperature, which generates a strong temperature slip upon reaching the boundaries. A difference in the wave characteristics exists between this ballistic regime and the transitional regime; in ballistic transport the equilibrium energy after the wavefront passes is almost the same as in the initial condition. This is because the hot phonons undergo almost negligible scattering and dissipate little energy while it travel through the domain. As a consequence, the peak temperature remains almost unchanged as it approaches to the boundary.

5.3. Comparison between gray LBM and other methodologies

5.3.1. Comparison with Fourier, Cattaneo, and ballistic-diffusive equations for thin film heating

Transient heat conduction across a thin film is simulated via the LBM and compared with several other governing equations: Fourier, Cattaneo, and the ballistic-diffusive equation (BDE) [6,7,19]. The initial temperature of the film is $T^* = 0$. At time $t^* = 0^+$, one end ($X^* = 1$) of the film is kept at the initial temperature ($T^* = 0$) while a higher temperature ($T^* = 1$) is imposed on the other end ($X^* = 0$). The transient heat conduction in the film is examined at various film thicknesses.

Fig. 7(a) shows transient temperature profiles for $Kn = 0.1$, transport within the diffusive regime. Results for the LBM are similar to those for the BDE, which itself is an approximation of the phonon BTE, with both approaches exhibiting clear diffusive behavior, owing to the large length and time scales. Both the Fourier and Cattaneo equations exhibited the diffusive temperature profiles which are in general agreement to those by the LBM and the BDE. However they failed to capture the temperature slip at the boundaries, due to non-equilibrium conditions at very short time scales, between the emitted and received phonons at the boundary.

In Fig. 7(b), transient temperature profiles for the transitional regime ($Kn = 1$) are provided. The LBM again shows a similar hot boundary temperature slip to that for the BDE but exhibit a higher temperature inside the domain exhibiting a more prominent ballistic

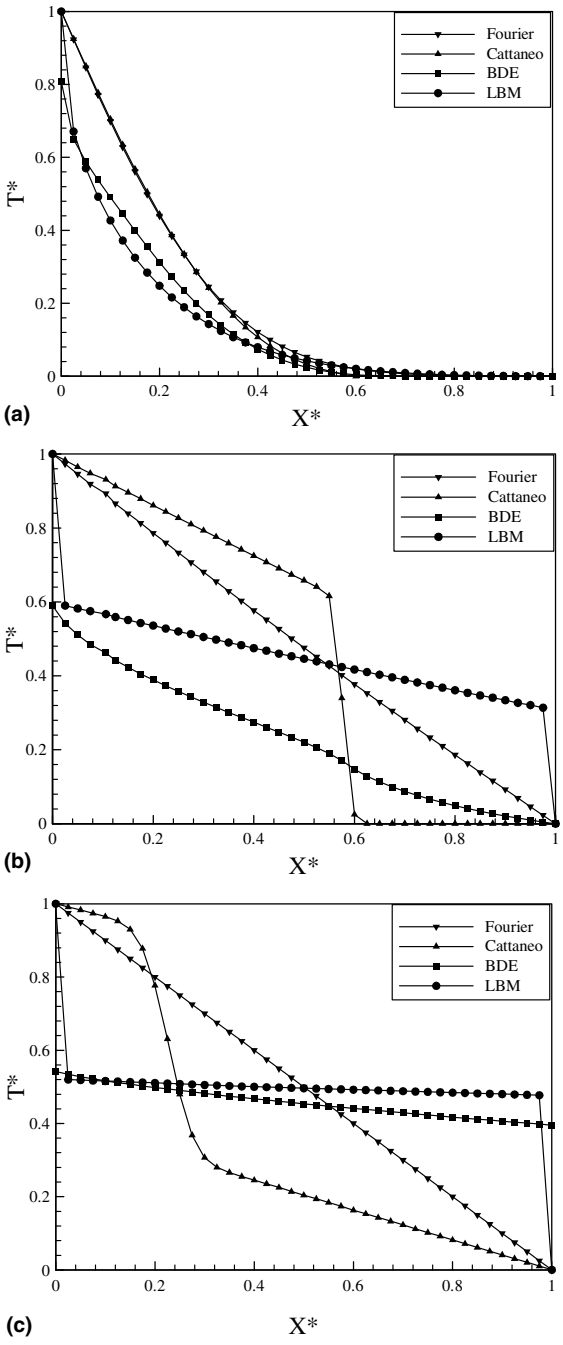

Fig. 7. Transient heat transport in a thin film for (a) $Kn = 0.1$ (diffusive regime) and $t^* = 10.0$; (b) $Kn = 1.0$ (transitional regime) and $t^* = 1.0$; and (c) $Kn = 10.0$ (ballistic regime) and $t^* = 1.0$.

behavior than BDE. Also the LBM shows a temperature slip at the cold boundary similar to the one at the hot boundary which the BDE fails to capture. As expected, both the Fourier and Cattaneo equations fail to describe the temperature profile characteristic of the transitional regime. The Fourier equation provides an linear profile without any temperature discontinuities at the boundaries, while the Cattaneo equation gives a wave-like behavior which does not exhibit temperature slip at the boundaries, and does not provide propagation to the cold boundary ($X^* = 1.0$), unlike the other methodologies.

Fig. 7(c) depicts the temperature distributions for a thin film within the ballistic regime. The temperature distribution for the LBM simulation is characterized by significant temperature slip conditions at each boundary, and ballistic transport inside the thin film without much decrease in the temperature, showing that the phonons do not undergo significant scattering processes, due to very small thickness of the film. Thus, phonons are unable to distribute their energy and remain at an almost constant energy level while traveling across the film. The BDE also captures the ballistic behavior as LBM with similar temperature jump at the hot boundary but exhibit a higher diffusive component resulting in more temperature drop across the film as compared to the LBM. The Fourier equation again shows a linear drop across the film thickness, with no temperature slip conditions at the boundaries, thus not capturing the ballistic transport of phonons whereas the Cattaneo equation exhibits reflection of the temperature wavefront from the cold boundary, which again is an unrealistic scenario, and it also fails to capture the temperature slip and ballistic transport of phonons. Thus, both Fourier and Cattaneo equations are unable to capture the sub-continuum behavior, indicating their inability to predict sub-continuum energy transport accurately.

5.3.2. Comparison with Fourier equation for SOI simulation

Here, we compare the peak hotspot temperature rise in an SOI simulation via the gray LBM with those obtained from the Fourier equation. The percentage (%) deviation is defined as

$$\%\ \text{deviation} = \left|\frac{\Delta T_{\text{LBM}} - \Delta T_{\text{Fourier}}}{\Delta T_{\text{Fourier}}}\right|, \tag{16}$$

where ΔT_{LBM} and $\Delta T_{\text{Fourier}}$ are the difference between the maximum hotspot temperature and the reference temperature ($T = 300$ K) obtained from the LBM solver and the Fourier equation solver, respectively.

These deviations can be better visualized by analyzing the temporal evolution of temperature at the center of the hotspot for both the LBM and Fourier solutions for each regime. Fig. 8(a) shows the time evolution of the temperature at the center of the hotspot obtained from both the LBM and the Fourier equation for $Kn = 0.01$ (diffusive regime). When the heat pulse is switched on, we observe a roughly linear temperature

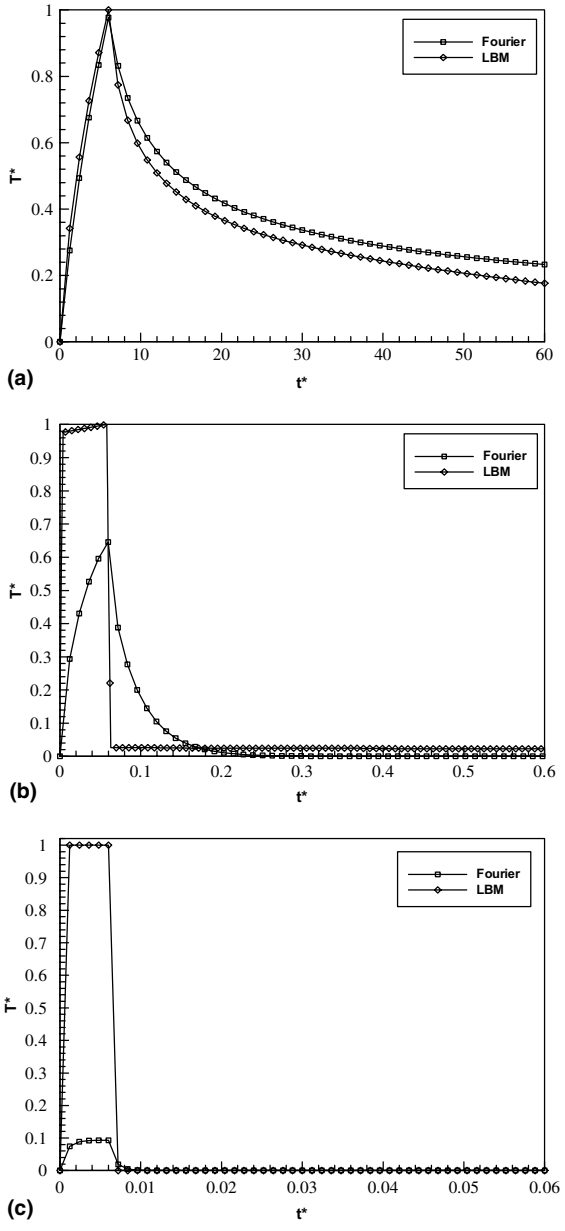

Fig. 8. Transient temperature profile at the center of the hotspot for Fourier equation and LBM solutions for (a) $Kn = 0.01$ (diffusive regime) with heat pulse duration $t_q^* = 0.6$; (b) $Kn = 1.0$ (transitional regime) with heat pulse duration $t_q^* = 0.006$; and (c) $Kn = 10$ (ballistic regime) with heat pulse duration $t_q^* = 0.0006$.

rise and the maximum temperatures predicted by both methods are within 2.5% of each other. After the pulse is turned off, the Fourier solution decays a little slower than the LBM solution, yet still follows the general trend.

The difference in the temporal temperature profile becomes conspicuous for $Kn = 1.0$ (transitional regime), as shown in Fig. 8(b). Both solutions provide a rapid increase when the pulse is turned on, with the LBM solution shows approximately 50% higher temperature than the Fourier equation prediction. But when the pulse is turned off both the approaches exhibits considerably different thermal relaxation, where as the Fourier equation predicts an exponential decrease, the LBM solution predicts a sudden fall in temperature due to the non-equilibrium nature of the heating followed by a slower relaxation of energy.

Similar behavior is again observed as the Kn is increased to 10, as shown in Fig. 8(c), which is in the ballistic transport regime. This regime has a highly non-equilibrium behavior with the LBM result showing almost an order of magnitude higher peak temperature rise than the Fourier equation predictions. This result is consistent with the observations made by many authors who have claimed that the Fourier equation underestimates the maximum temperature substantially as the we move towards sub-continuum (high Kn) regime and does not adequately capture the highest temperature levels present in sub-continuum energy transport, which is important in the design and operation of the next generation electronic devices, especially transistors.

6. Conclusions

A gray lattice Boltzmann method is developed for phonon transport under the Debye assumption, and employed to examine multi-length and -time scale heat conduction in thin films from continuum to sub-continuum regimes. The steady-state and transient results capture the characteristic temperature profiles in the diffusive, transitional, and ballistic regimes. A simplified model of an SOI transistor is used to predict the transient thermal response of the device to heat generation due to electron–phonon scattering. The LBM results agree very well with those of the Fourier, Cattaneo, and BD equations available in the literature [2,6,10,19,20]. As expected, both the Fourier and Cattaneo equations result in significantly different results than those of the LBM when the sub-continuum effects become dominant. It is considered that the LBM is capable of capturing the physics of heat conduction by phonon transport in multiple transport regimes, and thus can be used in the thermal design and modeling of sub-micron electronic devices e.g., SOI transistors. The LBM results reported here exhibit excellent agreement with other methodologies for their range of applicability, at a lesser computational effort, thus presenting itself as a valid, accurate numerical simulation tool for multi-length scale energy transport.

Acknowledgements

The authors gratefully acknowledge the support from the National Science Foundation grant CTS-0103082 and the ICES Pennsylvania Infrastructure Technology Alliance (PITA) Program sponsored by the Commonwealth of Pennsylvania's Department of Community and Economic Development.

References

[1] M.I. Flik, B.I. Choi, K.E. Goodson, Heat transfer regimes in microstructures, J. Heat Transfer 114 (1992) 666–674.
[2] A. Majumdar, Microscale heat conduction in dielectric thin films, J. Heat Transfer 115 (1993) 7–16.
[3] International Technology Roadmap for Semiconductors, ITRS 2003 update, http://public.itrs.net/.
[4] M. Kaviany, A.J.H. McGaughey, Integration of molecular dynamics simulations and Boltzmann transport equation in phonon thermal conductivity analysis, IMECE2003-41899, 2003.
[5] P.G. Sverdrup, Y.S. Ju, K.E. Goodson, Sub-continuum simulations of heat conduction in silicon-on-insulator transistors, J. Heat Transfer 123 (2001) 130–137.
[6] S. Narumanchi, J.Y. Murthy, C.H. Amon, Simulation of unsteady small heat source effects in sub-micron heat conduction, J. Heat Transfer 125 (2003) 896–903.
[7] D. Cahill, W. Ford, K.E. Goodson, G. Mahan, A. Majumdar, H. Maris, R. Merlin, S. Phillpot, Nanoscale thermal transport, J. Appl. Phys. 93 (2) (2003) 793–818.
[8] G. Chen, Particularities of heat conduction in nanostructures, J. Nanoparticle Res. 2 (2000) 199–204.
[9] G. Chen, Phonon heat conduction in nanostructures, Int. J. Therm. Sci. 39 (2000) 471–480.
[10] S.V. Narumanchi, J.Y. Murthy, C.H. Amon, Comparison of different phonon transport models in predicting heat conduction in sub-micron silicon-on-insulator transistors, J. Heat Transfer 127 (7) (2005) 713–723.
[11] S.V. Narumanchi, J.Y. Murthy, C.H. Amon, Sub-micron heat transport model in silicon accounting for phonon dispersion and polarization, J. Heat Transfer 126 (6) (2004) 946–955.
[12] W. Zhang, T.S. Fisher, Application of the lattice Boltzmann Method to Sub-continuum heat conduction, IMECE2002-32122, 2002.
[13] S.S. Ghai, R.A. Escobar, C.H. Amon, M.S. Jhon, Sub-continuum heat conduction in electronics using the lattice Boltzmann method, InterPack 2003-35258, 2003.
[14] R.A. Escobar, S.S. Ghai, M.S. Jhon, C.H. Amon, Time-dependent simulations of sub-continuum heat generation effects in electronic devices using the lattice Boltzmann method, IMECE2003-41522, 2003.
[15] S.S. Ghai, W.T. Kim, R.A. Escobar, C.H. Amon, M.S. Jhon, A novel heat transfer model and its application to information storage systems, J. Appl. Phys. 97 (2005) 10P703.
[16] C.L. Tien, A. Majumdar, F.M. Gerner, Microscale Heat Conduction, Taylor & Francis, Washington, DC, 1998.
[17] N.W. Ashcroft, N.D. Mermin, Solid State Physics, Harcourt, Fort Worth, TX, 1976.
[18] S. Succi, The Lattice-Boltzmann Equation for Fluid Dynamics and Beyond, Clarendon Press, Oxford, UK, 2001.
[19] G. Chen, Ballistic-diffusive equations for transient heat conduction from nano to macroscales, J. Heat Transfer 124 (2004) 320–328.
[20] A.A. Joshi, A. Majumdar, Transient ballistic and diffusive phonon heat transport in thin films, J. Appl. Phys. 74 (1) (1993) 31–39.